THORKILDSEN, G. (1987). *Acta Cryst.* A43, 361-369.
VIDAL-VALAT, G., VIDAL, J. P., KURKI-SUONIO, K. & KURKI-SUONIO, R. (1987). *Acta Cryst.* A43, 540-550.
WECKERT, E. & HÜMMER, K. (1990). *Acta Cryst.* A46, 387-393.
ZUO, J. M., GJØNNES, K. & SPENCE, J. C. H. (1989). *J. Electron Microsc. Tech.* 12, 29-33.
ZUO, J. M., HØIER, R. & SPENCE, J. C. H. (1989). *Acta Cryst.* A45, 839-855.
ZUO, J. M. & SPENCE, J. C. H. (1991). *Ultramicroscopy*, 35, 185-193.
ZUO, J. M., SPENCE, J. C. H. & HØIER, R. (1989). *Phys. Rev. Lett.* 62, 547-550.

Acta Cryst. (1993). A49, 429-435

Automated Structure-Factor Refinement from Convergent-Beam Electron Diffraction Patterns

BY J. M. ZUO

Physics Department, Arizona State University, Tempe, AZ 85287, *USA*

(*Received* 29 *June* 1992; *accepted* 13 *October* 1992)

Abstract

An improved algorithm is described for automated structure-factor refinement using convergent-beam electron diffraction patterns. In addition to refinement of structure factors, absorption coefficients and sample thickness, the new algorithm includes beam-direction refinement, the inclusion of weak-beam effects using the Bethe potential and the inclusion of finite-sized detector effects. The use of these new features is illustrated through the refinement of the MgO 200 systematic reflections.

1. Introduction

Convergent-beam electron diffraction (CBED) is a highly efficient structural probe - a large amount of quantitative structural and compositional information may be obtained from volumes as small as 1 nm in diameter. There has been continuous interest recently in devising systematic methods to extract this information from the readily available CBED patterns (for a recent review, see Spence, 1993). Most recently, Zuo & Spence (1991) used numerical optimization methods to automate the process of comparing elastic-filtered CBED intensities with Bloch-wave calculations, while treating structure factors, absorption coefficients and thickness as adjustable parameters. Similar methods may be used to compare experimental high-order Laue-zone (HOLZ) patterns with kinematical simulations, with the lattice parameters treated as adjustable parameters (Zuo, 1992*a*). The structure factors give compositional and structural information on the crystal, while the lattice parameters give local strain information. There have been many other efforts to extract information from CBED patterns using optimization methods. These include the theoretical studies by Marthinsen, Høier & Bakken (1990) on the refinement of structure-factor amplitude and phase from non-systematic CBED patterns, studies by Bird & Saunders (1992) on the possibility of determining crystal structure from zone-axis CBED patterns, and the experimental measurement of atomic positions from zone-axis HOLZ intensities by Tanaka & Terauchi (1990). The earlier automated refinement method described by Zuo & Spence (1991) was effective in refining complex structure factors and thickness, but required tedious precise orientation matching and has since been improved in several ways. These include an algorithm for automated beam-direction refinement, which was not available previously. The other new feature is a modification of the original algorithm to allow weak beams to be treated by the Bethe-potential method (Bethe, 1928). The Bethe-potential method was chosen over the perturbation method (Eaglesham, 1989; Zuo, 1991) because it has the advantages of simplicity and speed (Zuo, 1992*b*). This new feature allows us to include weak beams in the simulation to improve the convergence and requires only a fraction of the computer time compared to diagonalizing a full matrix with the weak beams included. The third new feature is an algorithm to include detector effects in the simulation and thus reduce possible systematic errors in the measured experimental data. These new features will be discussed in the following sections. Before doing so, the results of earlier work will be briefly summarized.

In a previous paper (Zuo & Spence, 1991), the algorithm *REFINE/CB* was described for automation of the process of measuring structure factors, absorption coefficients and thickness from energy-filtered convergent-beam electron diffraction data in the systematics orientation. This was accomplished by the definition of a best-fit parameter (χ^2) and use

0108-7673/93/030429-07$06.00

of an optimization routine to find the lowest χ^2 - the best fit. Automation of this process: (1) speeds up the whole process; (2) avoids systematic errors due to subjectivity; and (3) simplifies the method. χ^2 is defined similarly to the standard definition of the goodness-of-fit parameter in statistics,

$$\chi^2 = \sum_i (f_i/\sigma_i^2)(CI_i^{\text{theory}} - I_i^{\text{exp}})^2 \quad (1)$$

and

$$C = \left[\sum_i (f_i/\sigma_i^2) I_i^{\text{exp}} I_i^{\text{theory}}\right] \Big/ \left[\sum_i (f_i/\sigma_i^2) I_i^{\text{theory}} I_i^{\text{theory}}\right]. \quad (2)$$

Here, σ_i^2 is the variance, which can be found from repeated measurements or using $\sigma_i^2 = I_i^{\text{exp}}$ with the assumption of Poisson statistics for electron counting with a detector quantum efficiency (DQE) of 1. The f_i are weight coefficients, which are usually set to 1 or 0: 1 for points inside the convergent-beam disc and 0 for those outside. The f_i can also be adjusted to increase the importance of particular intensity points to χ^2, which may be sensitive to particular parameters. However, this weighting must be used with great caution since the variance at the point is reduced by increasing f_i. χ^2 is the same as the R factor used in X-ray refinement if f_i are set to 1 or 0 [for a definition of the R factor, see, for example, Cruickshank (1969)]. The experimental intensity data are assumed to consist of elastic energy-filtered parallel-line scans (see Fig. 1). The scan coordinates are the coordinates of points 1, 2 and 3 of Fig. 1 in units of the two basis vectors **g** and **h**. The parameters of structure-factor amplitude and phase, absorption coefficients and phases, and thickness are adjusted to find the lowest χ^2. The theoretical intensity is calculated by the Bloch-wave method (Zuo, Gjønnes & Spence, 1989) and perturbation theory (Zuo, 1991). Perturbation theory is used when the changes in the structure factors and absorption coefficients are smaller than a previously entered limit. The use of the perturbation method results in a saving of computing time proportional to the number of beams included in the calculation. The optimization method used in this program is the simplex method. This optimization routine is more dynamic than other routines reported although the convergence to the minimum is slower. The whole process is thus rather similar to the Rietveld method in neutron diffraction (Rietveld, 1969).

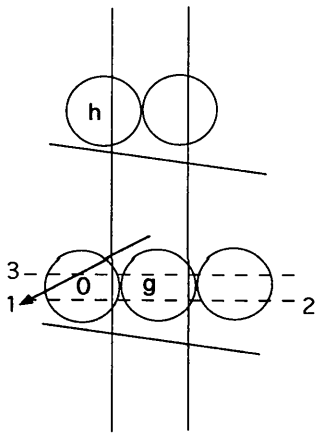

Fig. 1. The beam direction is defined by a vector from the center of the Laue circle to a point in the diffraction pattern. Points 1, 2 and 3 and the dashed lines define the parallel-line scans used in the experiment. The solid lines are the Kikuchi lines associated with **g** and **h**. The disc is a CBED disc.

2. Automated beam-direction refinement

The beam direction describes the orientation relationship between the crystal and the incident plane wave. It is needed for the interpretation of diffraction patterns. Accurately measured beam directions are especially important in quantitative electron diffraction because of the sensitivity of dynamical electron diffraction to the beam direction. In a diffraction pattern, each point is a new beam direction. Following the convention described by Zuo & Spence (1991), the beam direction is specified by the component of a wave vector in the zero-order Laue-zone (ZOLZ) plane, $\mathbf{K}_t$, originating from the center of the Laue circle. This vector is described by its components in terms of the base vectors **g** and **h** (see Fig. 1). In a CBED pattern, however, only a point in the zero disc is truly an incident-beam direction; a point in the diffracted disc **g** is related to a point in the zero disc by a displacement vector $-\mathbf{g}$. The experimental intensity is measured along a set of parallel lines. The coordinates of these parallel lines are defined by points 1, 2 and 3 as shown in Fig. 1. A total of n equally spaced points on each line and m lines are measured. The beam directions for points 1, 2, 3 and the center of the zero disc, $\mathbf{K}'_{t1}$, $\mathbf{K}'_{t2}$, $\mathbf{K}'_{t3}$ and $\mathbf{K}'_{t0}$, are also measured. (The prime is used to distinguish $\mathbf{K}'_t$ from $\mathbf{K}_t$, the incident-beam direction in the zero CBED disc.) Then the beam direction of the ith point on the jth line is

$$\mathbf{K}'_t = (i-1)(\mathbf{K}'_{t2} - \mathbf{K}'_{t1})/(n-1) + (j-1)(\mathbf{K}'_{t3} - \mathbf{K}'_{t1})/(m-1).$$

The incident-beam direction at this point is

$$\mathbf{K}_t = \mathbf{K}'_t \quad \text{if } |\mathbf{K}'_t - \mathbf{K}'_{t0}| < d/2,$$

$$\mathbf{K}_t = \mathbf{K}'_t - \mathbf{g} \quad \text{if } |\mathbf{K}'_t - \mathbf{K}'_{t0} - \mathbf{g}| < d/2$$

or non-existent for those points outside the CBED disc. Here, d is the diameter of the CBED disc in units of Å^{-1}. Thus, the incident-beam direction for each scan point is uniquely determined by the beam direction at points 1, 2, 3 and at the center of the zero disc. The beam-direction refinement depends on

features that are sensitive to the beam direction. For example, the deficency and excess of intensity in the zero disc and in a systematic disc g are used to refine the component of the beam direction along the systematic orientation. The deficiency in the zero disc caused by non-systematic reflections is used to refine the component of the beam direction normal to the systematic orientation.

Automation of the beam-direction refinement is done using the previous definition of χ^2 and the 'simplex' optimization method. The algorithm is implemented in subroutine *BEAMRF*, which can be called before the structure-factor refinement. In this algorithm, the adjustable parameters are the crystal thickness and the x and y components of the incident electron wave vector at points 1, 2, 3 and at the center of the zero disc (see Fig. 1). Fig. 2(a) shows a simplified flow chart of this subroutine, while Fig. 2(b) shows the flow chart of subroutine *TREF* called by *BEAMRF* to find the lowest χ^2 for a particular set of beam directions with thickness as the adjustable parameter. The beam-direction refinement routine is not designed to search for beam directions from one zone axis to another; it is intended to refine the beam direction as measured approximately from diffraction patterns recorded on film. These measurements are based on the geometry of HOLZ lines or Kikuchi lines, using methods described by Spence & Zuo (1992). New efforts are under way to develop an object-oriented Apple Macintosh program to simulate geometric diffraction patterns showing Kikuchi and HOLZ lines, with the microscope x and y tilt under active control. This will enable instant diffraction-pattern indexing and initial beam-direction measurement. These data can be transferred to the *REFINE/CB* program for further structure-factor refinement.

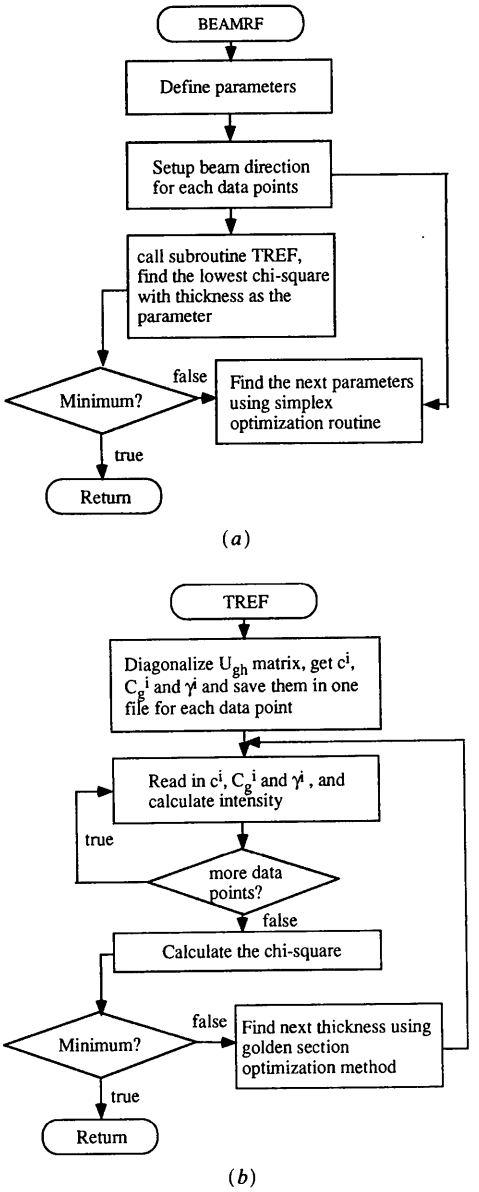

Fig. 2. (a) A simplified flow chart of subroutine *BEAMRF*. The parameters refined here can be the coordinates of points 1, 2 and 3 and the center of the zero disc (see Fig. 1). (b) Flow chart of subroutine *TREF* called by *BEAMRF* to find the lowest χ^2 for the particular beam direction with the thickness as the adjustable parameter.

3. Inclusion of weak beams by the Bethe-potential method

The possibility of using Bethe perturbation potentials to include weak beams has been demonstrated by a number of authors (see, for example, Gjønnes, Gjønnes, Zuo & Spence, 1989). This method was chosen over the perturbation method for the refinement procedure because of its accuracy and speed.

In the Bloch-wave method, the wave field inside the crystal is a composite of different Bloch waves,

$$\Psi(r) = \sum_i c_i \exp\left[2\pi i(\mathbf{K} + \gamma^i \mathbf{n}) \cdot \mathbf{r}\right] \times \sum_{\mathbf{g}} C_{\mathbf{g}}^i \exp\left(2\pi i \mathbf{g} \cdot \mathbf{r}\right). \quad (3)$$

The Bloch-wave function is found by solution of the following dispersion equation:

$$2KS_g C_g + \sum_h U_{gh} C_h = 2K_n \gamma C_g. \quad (4)$$

Here, γ^i and C_g^i are eigenvalues and eigenvectors, c^i is the excitation coefficient of the ith Bloch wave and S_g is the excitation error for reflection g. [For an introduction to the Bloch-wave method, see Spence & Zuo (1992).] Equation (4) is an eigenvalue equation. The dimension of the equation is the number n of beams included. The solution is obtained by a numerical matrix diagonalization. The computing

time and memory required for the diagonalization is proportional to n^2. Thus, in practice, the number of beams included in the simulation must be limited. The truncation of beams may introduce a systematic error if the calculation fails to converge. This is illustrated in Fig. 3, in which the thickness *Pendellösung* for an MgO crystal along the [001] zone axis is calculated using different numbers of beams in the ZOLZ only. No absorption or Debye–Waller factors were used. Atomic scattering factors for neutral spherical Mg and O atoms were used, with $a = 4.2112$ Å. The computing time using a VAXstation 3200 is shown in Table 1. Fig. 4 shows a comparison between the Bloch-wave calculation with $n = 177$ and a multislice calculation with 1394 beams included. This shows that $n = 177$ is sufficient to achieve convergence in this case. For other incident-beam directions or other crystals, this number may be larger or smaller. In the automated structure-refinement procedure for CBED, each data point is a new beam direction and a separate diagonalization is required and this calculation is repeated for each step in the search for the lowest χ^2. For merely 100 data points and 100 search steps, the total computing time will be 10 000 times the single diagonalization time. For the $n = 177$ diagonalization, the total time will be 1550 h according to Table 1 and the above calculations. Hence, such computation is impractical with today's computers. Of the 177 beams included in the calculation, the majority are weak beams. A beam h is said to be a weak beam if (Zuo, 1991)

$$2KS_h \gg |U_g|_{\max}, \tag{5}$$

where $|U_g|_{\max}$ is the largest $|U_g|$ involved. For those Bloch waves associated with strong beams, the eigenvalue γ is of the order of the interaction U_g. In these Bloch waves, the equation for the weak beam h may be approximated by

$$2KS_hC_h + \sum_g U_{hg}C_g \simeq 0.$$

Thus,

$$C_h \simeq -\sum_g U_{hg}C_g/2KS_h. \tag{6}$$

Substituting this into (4) for the strong beams, we obtain

$$\left(2KS_g - \sum_{h\neq g,g'} |U_{gh}|^2/2KS_h\right) C_g + \sum_{g'\neq g,h} \left(U_{gg'} - \sum_{h\neq g,g'} U_{gh}U_{hg'}/2KS_h\right) C_{g'} = 2K\gamma C_g, \tag{7}$$

where the h summation is over all the weak beams and the g' summation is over all the strong beams. The correction terms in (7) are called Bethe potentials. The Bethe potential actually has two terms: one is a correction term for the excitation error, the other is the correction for the structure factor. Both are important. Calculation of the Bethe potentials is straightforward. Once they are calculated, a matrix containing only strong beams with the modified structure factors

Table 1. *Computing times and conditions for curves (a) to (e) in Figs. 3 and 5*

n is the number of beams treated by diagonalization; $N - n$ is the number of weak beams treated by the Bethe potential.

Curve	n	$N-n$	CPU time (s)
(*a*)	177	0	558
(*b*)	89	0	107
(*c*)	45	0	31.2
(*d*)	21	0	12.6
(*e*)	45	132	47.7

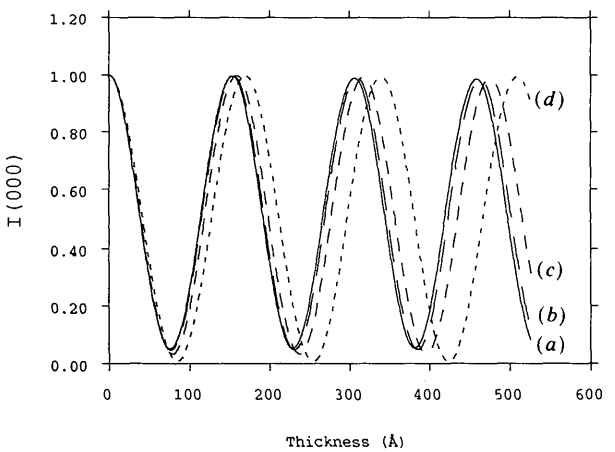

Fig. 3. Calculated *Pendellösung* intensities for MgO along [001] with different numbers of beams: 177 for curve (*a*); 89 for curve (*b*); 45 for curve (*c*); and 21 for curve (*d*).

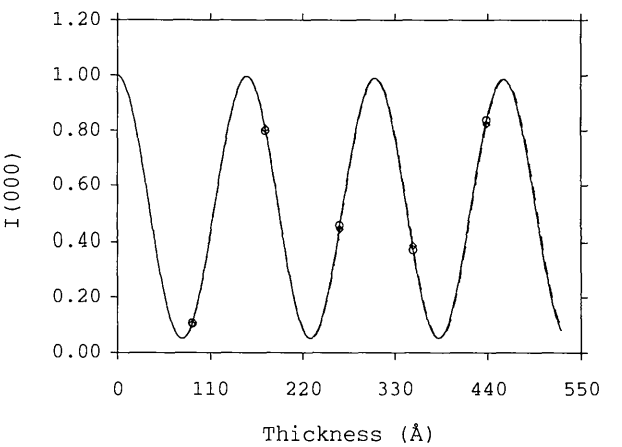

Fig. 4. Comparison between *Pendellösung* intensities calculated by the Bloch-wave method using 177 beams (dashed) line and by the multislice method with 1394 beams (solid line). The circles and diamonds mark selected points on these two curves.

and excitation errors is diagonalized. The eigenvalues and eigenvectors obtained are used for the intensity calculations. The diagonalization time will be proportional to the square of the number of strong beams, not the total number of beams, and the calculation of the Bethe potential is proportional to the number of weak beams, not the square of this number. This can save considerable computer time compared to straightforward diagonalization. Let us suppose that a total of N beams are included, among which n beams are strong and $N-n$ are weak. In the Bethe-potential method, the $n \times n$ matrix containing all the strong beams is diagonalized and the Bethe potential is calculated for each element in this submatrix. The computer time for doing this is proportional to $cn^2 + n^2(N-n)/2$, compared to a computer time of cN^2 for full diagonalization, where c is a coefficient much larger than 1. Fig. 5 shows the results of using the Bethe potential with $n=45$ and $N=177$, in comparison with the exact calculations for $N=n=177$ or 45, which is sufficiently close to the results of matrix diagonalization with 177 beams. The computing time using the Bethe potential is only slightly higher than the matrix diagonalization with 45 beams.

In the implementation of the Bethe-potential method in the automated refinement procedure, the practical question arises as to which beam should be considered as a weak beam. This choice depends on the beam direction. The criterion

$$S_g > S_{g\max} \tag{8}$$

is used to define a weak beam. The cutoff $\mathbf{S}_{g\max}$ is a parameter in the algorithm, which may be varied. It is generally recommended that $2KS_{g\max} \geq 1.0$ Å^{-2}. For each incident-beam direction, *REFINE/CB* calculates the excitation error for each beam and chooses the weak beams and strong beams based on

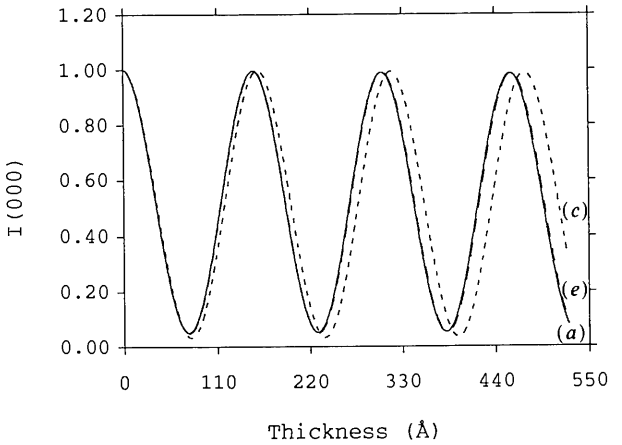

Fig. 5. Comparison between *Pendellösung* intensities calculated with $n=177$ and $N-n=0$ (curve a), $n=45$ and $N-n=0$ (curve c) and $n=45$ and $N-n=132$ (curve e). For details, see text.

(8). The other method of treating weak-beam effects is the perturbation approach (Eaglesham, 1989; Zuo, 1991). The computation in the perturbation approach requires the evaluation of a second-order correction to the eigenvalues and a first-order correction to the eigenvectors. The computing time is thus proportional to $cn^2 + n^3(N-n)$, which is slower than the Bethe-potential method. In the auto-refinement procedure, only the intensity of the 'strong beams' can be calculated. To prevent the algorithm from treating a reflection in the scan as a weak beam, we define a parameter NCORE. The first NCORE beams will always be treated by diagonalization only. To test the accuracy of the Bethe-potential method, we have calculated a systematic rocking curve in a sparse zone axis by full diagonalization only and then used this as test 'experimental data' for a refinement, in which beams with $2KS_{g\max} \geq 1.0$ Å^{-2} are treated by the Bethe-potential method. The refined structure factors and absorption coefficients are the same as those used in the test rocking-curve calculation. Hence, the possible systematic error owing to use of the approximate Bethe-potential method is zero in this case. Again, this result depends on the crystal and orientations used. In practice, $S_{g\max}$ may be varied to see if it gives different refined parameters. This should be repeated until results are the 'same' in terms of the estimated errors.

4. Detector effects

This refers to the effects of the finite-sized detector on the measured rocking curve, and hence its effects on the results of the structure-factor refinement. This was previously ignored in our earlier publication (Zuo & Spence, 1991). The detector effect may be generalized to include the beam broadening due to the dispersion in the electron–photon converter, such as yttrium aluminium garnet (YAG), used in the two-dimensional charge-coupled device (CCD) detection array, or the diffuse scattering of thermal inelastic scattering or of random structural disorder such as that due to disorder occupancy. The detector effect on the rocking curve is the convolution of the ideal rocking curve with the detector response. The detector function can be a Gaussian-type distribution function in the case of diffuse scattering or a function of 1 inside the detector aperture and 0 outside. For a circular detector, the response function of the detector for a one-dimensional systematic scan is $2(D^2-d^2)^{1/2}$ for $d<D$ and 0 for $d \geq D$, where D is the detector radius and d is the distance to the center of the detector. This assumes that the intensity in a direction normal to the systematic direction is constant. In the general case of a two-dimensional diffraction pattern, a two-dimensional convolution with the detector function is required. Deconvolution of the experimental data against the detector response function is often difficult because of the noise in the experimental

data and the noise-amplification effects of the deconvolution process. Thus, it is better to convolute the theoretical data with the detector response function to simulate the experimental conditions. The convolution is done numerically using the fast Fourier transformation. In this way, different response functions can be accommodated easily. In the experimental measurement, the spacing of points should be comparable to the size of the detector, since it is a waste of both computing and experimental-instrument time to have a spacing much smaller than the detector size. The rocking curve is magnified using numerical interpolation and reduced after the convolution. The detector generally affects the high-order beams most because of the rapidly varying features in the rocking curve of these beams. This is illustrated in the refinement of the 200 and 400 structure factors of MgO with and without taking account of detector effects, described in the next section.

5. An example

Fig. 6 shows an example of structure-factor refinement using the improved *REFINE/CB* program. The energy-filtered experimental data are for MgO [200] systematics taken near the [012] zone axis at 100 kV from a Philips 400T microscope equipped with a serial energy-loss spectrometer tuned to the elastic peak. The MgO crystal is a rectangular plate of MgO smoke. The detector size is 0.167 mrad. The final refinement was carried out with a 123 beam refinement and $2KS_{gmax} = 1.0$ Å^{-2}. Those beams with excitation errors larger than 1.0 were treated by the Bethe-potential method. The structure factors involved other than those being refined were calculated from atomic scattering factors of neutral Mg and O atoms as listed in Table 2.2*B* of *International Tables for X-ray Crystallography* (1974). The Debye-Waller factors used for the Mg and O atoms are 0.346 and 0.315 Å^2, respectively, from neutron diffraction measurement (Sabine, Von Dreele & Jorgensen, 1988). These Debye-Waller factors were also used to calculate those absorption coefficients not being refined, using subroutine *ATOM* (Bird & King, 1990). The experimental detector size was used to simulate the detector effect. The final results are shown in Fig. 6, and the refined structure factors are

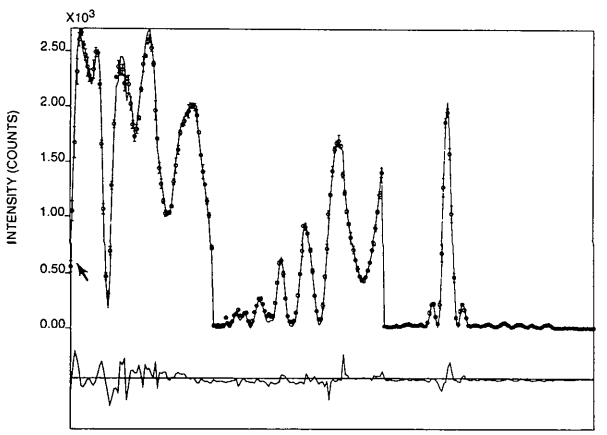

Fig. 6. Results of MgO 200 systematics refinement using the improved *REFINE/CB* program. The circles with error bars are the experimental data and the upper solid line is the best fit. The lower solid line is the difference between the experimental data and the theoretical best fit.

$$\chi^2 = 7.7$$
$$U(200) = 0.05551\ (8)\ \text{Å}^{-2},$$
$$U'(200) = 0.001381\ (40)\ \text{Å}^{-2}$$
$$U(400) = 0.02488\ (30)\ \text{Å}^{-2},$$
$$U'(400) = 0.00045\ (6)\ \text{Å}^{-2},$$
$$t = 953.5\ (9)\ \text{Å}.$$

In Fig. 6, the deficiency in the zero disc due to the 400 Bragg condition and the corresponding excess in the 400 disc were used for initial estimation of the x component of the beam direction and are the features exploited in the auto-refinement of three-dimensional beam directions. The deficiency indicated by the arrow in Fig. 6 is due to the $4\bar{4}2$ Bragg condition, which is used for the y component of beam-direction measurement and refinement.

The same refinement with a detector of negligible dimensions gives

$$\chi^2 = 8.0,$$
$$U(200) = 0.05555\ \text{Å}^{-2},$$
$$U'(200) = 0.001392\ \text{Å}^{-2},$$
$$U(400) = 0.02466\ \text{Å}^{-2},$$
$$U'(400) = 0.00042\ \text{Å}^{-2},$$
$$t = 953.5\ \text{Å}.$$

The value of χ^2 has increased slightly and there is significant difference in the measured 400 structure factor, but negligible difference in the 200 structure factor. In the diffuse-scattering case, the detector effects may become serious and must be included in the simulation.

The importance of the weak beams is illustrated by a repetition of the refinement with only 19 beams. This refinement gives

$$\chi^2 = 9.0,$$
$$U(200) = 0.05555\ \text{Å}^{-2},$$
$$U'(200) = 0.001311\ \text{Å}^{-2},$$
$$U(400) = 0.02535\ \text{Å}^{-2},$$
$$U'(400) = 0.00051\ \text{Å}^{-2},$$
$$t = 953.7\ \text{Å}.$$

The value of χ^2 has increased. In this case, the beam cut-off has a large effect on the 400 structure factor and absorption, and negligible effect on the other parameters. Zuo & Spence (1991) gave $U(200) = 0.05847$ Å^{-2} and $U(400) = 0.02484$ Å^{-2} at 120 kV or $U(200) = 0.05661$ Å^{-2} and $U(400) = 0.02405$ Å^{-2} at 100 kV. The reason for the difference between the current and previous values may be due to the difference in the data-normalization method used. The previous refinement used a point for normalization and particular weights were applied for intensities near the Bragg condition, while the current refinement uses $f_i = 1$ for every experimental point and uses (2) to calculate the normalization coefficients C. This is under further investigation. This, and a comparison with other studies on MgO, will be published in a forthcoming paper.

6. Concluding remarks

Features of the *REFINE/CB* program for the quantitative analysis of CBED patterns are:

1. dynamic beam-direction refinement using the simplex optimization method;
2. structure-factor amplitude and phase, absorption amplitude and phase, and thickness refinement using data collected along a line;
3. electron scattering intensity simulation by the three-dimensional Bloch-wave method;
4. weak beams included using the Bethe-potential method;
5. intensity calculation by the perturbation method for small changes in the scattering potential (*e.g.* owing to bonding effects);
6. error analysis.

The *REFINE/CB* program has been proved to be accurate and flexible in the examples provided and other applications, *e.g.* structure-factor phase determination in acentric crystals (Zuo, Spence, Downs & Mayer, 1993).

Recently, a method has also been developed for the automated refinement of lattice parameters from HOLZ-line patterns and for auto-generation of geometric diffraction patterns using only crystal data and the microscope x, y tilt as input. These methods and the *REFINE/CB* method have now become useful 'tools' available to extract both structural and compositional information from materials studied by convergent-beam electron diffraction, which has been traditionally underutilized. In the future, these methods can be integrated together with a user-friendly human interface. They can then be used like any of the many 'functions' on the microscope.

This work was supported by NSF Grant DMR-9015867 and NSF-ASU National Center for HREM. The author acknowledges many useful discussions with Professor J. C. H. Spence.

References

BETHE, H. A. (1928). *Ann. Phys. (Leipzig)*, **87**, 55-129.
BIRD, D. & KING, Q. A. (1990). *Acta Cryst.* A**46**, 202-208.
BIRD, D. & SAUNDERS, M. (1992). *Acta Cryst.* A**48**, 555-562.
CRUICKSHANK, D. W. J. (1969). *Crystallographic Computing*, edited by F. R. AHMED, pp. 187-197. Copenhagen: Munksgaard.
EAGLESHAM, D. J. (1989). 47th Annu. Proc. Electron Microscopy Society of America, pp. 482-483.
GJØNNES, K., GJØNNES, J., ZUO, J. M. & SPENCE, J. C. H. (1989). *Acta Cryst.* A**44**, 810-820.
International Tables for X-ray Crystallography (1974). Vol. IV. Birmingham: Kynoch Press. (Present distributor: Kluwer Academic Publishers, Dordrecht.)
MARTHINSEN, K., HØIER, R. & BAKKEN, L. (1990). *Proc. 12th International Congress on Electron Microscopy*, pp. 492-493. San Francisco Press.
RIETVELD, H. M. (1969). *J. Appl. Cryst.* **2**, 65-71.
SABINE, T. M., VON DREELE, R. B. & JØRGSEN, J.-E. (1988). *Acta Cryst.* A**44**, 374-379.
SPENCE, J. C. H. (1993). *Acta Cryst.* A**49**, 231-260.
SPENCE, J. C. H. & ZUO, J. M. (1992). *Electron Microdiffraction.* New York: Plenum.
TANAKA, M. & TERAUCHI, M. (1990). *Proc. 12th International Congress on Electron Microscopy*, pp. 518-519. San Francisco Press.
ZUO, J. M. (1991). *Acta Cryst.* A**47**, 87-95.
ZUO, J. M. (1992*a*). *Ultramicroscopy.* **41**, 211-223.
ZUO, J. M. (1992*b*). 50th Annu. Proc. Electron Microscopy Society of America, Part 2, pp. 1450-1451.
ZUO, J. M., GJØNNES, J. & SPENCE, J. C. H. (1989). *J. Electron Microsc. Tech.* **12**, 29-55.
ZUO, J. M. & SPENCE, J. C. H. (1991). *Ultramicroscopy*, **35**, 185-196.
ZUO, J. M., SPENCE, J. C. H., DOWNS, J. & MAYER, J. (1993). *Acta Cryst.* A**49**, 422-429.